J. Am. Soc. Mass Spectrom. (2018) 29:1331–1334
DOI: 10.1007/s13361-018-1948-4

APPLICATION NOTE

Gas-Phase Chemistry of Arylimido-Functionalized Hexamolybdates $[Mo_6O_{19}]^{2-}$

Jie Cao, QianQian Wang, Chang Liu, ShuQi An

Key Laboratory of Cluster Science, Ministry of Education of China, Beijing Key Laboratory of Photoelectronic/Electrophotonic Conversion Materials, School of Chemistry, Beijing Institute of Technology, Beijing, 100081, China

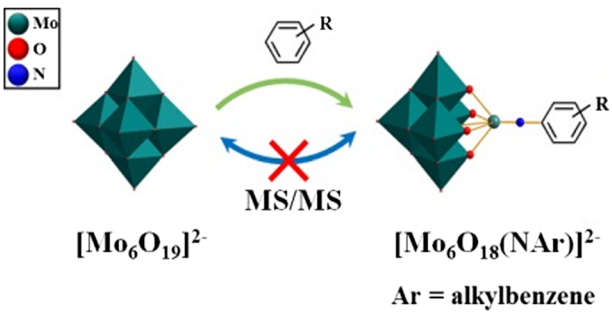

Abstract. The gas-phase fragmentations of a series of arylimido derivatives of hexamolybdate $[Mo_6O_{18}(NC_6H_{5-n}R_n)]^{2-}$ (**2–10,** where R = CH_3, i-C_3H_7, OCH_3, NO_2; n = 1 or 2) versus the parent species $[Mo_6O_{19}]^{2-}$ (**1**) were systematically studied using electrospray tandem mass spectrometry (ESI). Fragmentation of **1** generates two molybdate fragments only, $[Mo_3O_{10}]^{2-}$ and $[Mo_4O_{13}]^{2-}$, whereas decomposition of **2–10** went through two dissociation pathways in which path A generates a variety of molybdate fragments via breaking the Mo–N bond followed by the cleavages of the multiple Mo–O bonds, whereas path B produces a range of molybdate fragments with arylimido group via breaking the multiple Mo–O bonds on POM framework. Moreover, the presences of mixed-oxidation-state molybdate fragments are characteristic for the fragmentation. The gas-phase stability order obtained by energy-variable collision-induced dissociation (CID) experiment reveals that **2–10** are generally less stable than **1** and substitution on the benzene ring exerts a considerable effect on the stabilization of the hybrid clusters.

Keywords: Polyoxometalates, Arylimido derivatives, Gas-phase fragmentation

Received: 13 January 2018/Revised: 18 March 2018/Accepted: 18 March 2018/Published Online: 18 April 2018

Introduction

Polyoxometalates (POMs) are metal oxide clusters of early transition metals (Mo, W, V, Nb, Ta, etc.) that are typically observed in their highest oxidation states. POMs present unique structural and electronic properties that make them attractive for applications in many fields [1, 2]. Surface modification of POMs by covalent bonds via replacing/derivatizing the oxo ligands to develop POM-based inorganic/organic hybrid materials has attracted increasing attention because the covalent bond improves the stability of the hybrid assemblies and might enhance the interaction between the inorganic and organic components. These covalently functionalized POMs not only enrich POM structures but also diversify its properties for various applications [3–5]. Organoimido derivatives of the hexamolybdate ion, $[Mo_6O_{19}]^{2-}$, where the six terminal oxygen ligands in the hexamolybdate anion can be partially or completely replaced with arylimido ligands to give rise to polysubstituted derivatives with the general formula $(TBA)_2[Mo_6O_{(19-x)}(NAr)_x]$ (x = 1–6; $TBA^+ = (n\text{-}C_4H_9)_4N^+$, Ar = alkylbenzene), have drawn particular attention in recent years due to their unique structural feature, containing a delocalized π system onto POMs. The arylimido derivatives of POMs with a remote organic functional group can be utilized as building blocks to construct more complicated and interesting POM-organic hybrids.

Although a great number of organo-functionized POMs has been successfully synthesized so far [6–10], a systematic study of the gas-phase fragmentation of these organic/inorganic hybrid clusters has yet to appear. Fragmentation reflects the intrinsic structural feature where no solvent effect exists and provides insight into the favored decomposition pathways of gas-phase clusters. Fragmentation of the bare polyoxoanions including $[W_6O_{19}]^{2-}$, $[Mo_8O_{26}]^{4-}$, $[W_{10}O_{32}]^{4-}$, $[PW_{12}O_{40}]^{3-}$, $[SiMo_{12}O_{40}]^{4-}$, $[PMo_{12-n}W_nO_{40}]^{3-}$ (n = 0–12), and a series of polyoxovanadates [11–16] has been examined; however, this may

Electronic supplementary material The online version of this article (https://doi.org/10.1007/s13361-018-1948-4) contains supplementary material, which is available to authorized users.

Correspondence to: Jie Cao; *e-mail:* jcao@bit.edu.cn

not necessarily represent the fragmentation behavior of organo-functionized POMs where organic compounds are covalently grafted onto POMs' framework.

Herein, we report a systematic investigation on the gas-phase fragmentation of a series of arylimido hexamolybdate derivatives with a general formulae of $[Mo_6O_{18}(NC_6H_{5-n}R_n)]^{2-}$ (R = CH_3, i-C_3H_7, OCH_3, NO_2; n = 1 or 2) and the gas-phase stability study with an aim to probe the substitution effect on the stability of whole clusters. The "bare" hybrid POMs without the presence of other cations such as H^+ or TBA^+ were chosen for fragmentation and stability studies. Trends in the fragmentation pathways observed are described. The results are useful in defining further the scope of ESI-MS and CID in the characterization of POM-based organic/inorganic hybrid clusters. To the best of our knowledge, this was the first systematic study on the organo-functionalized POMs.

Experimental

Synthesis

Lindqvist POM **1** and its organoimido derivatives **2**–**10** were synthesized according to the literatures [17, 18], respectively.

ESI-MS Experiments

All electrospray ionization mass spectrometry (ESI-MS) measurements were performed on an Agilent 6520 Q-TOF LC/MS mass spectrometer, equipped with a quadropole and a time-of-flight (Q/TOF) mass analyzers for MS analysis. Solutions of **1**–**10** were prepared by dissolving in HPLC grade CH_3CN to a concentration of ca. 1×10^{-4} mol L^{-1}. 10 μL aliquot was removed and made up to 1 mL with CH_3CN to produce a 1×10^{-6} mol L^{-1} dilution suitable for MS testing. All samples were injected directly via an autosampler with a flow rate of 0.2 mL min^{-1}. The dual-spray electrospray ionization source condition was as follows: V_{cap}, 3500 V; skimmer, 65 V; OCT R_fV, 750 V; drying and nebulizer gas, N_2; nebulizer, 30 psi; drying gas flow, 10 L min^{-1}; drying gas temperature, 300 °C; fragmentor, 80 V; scan range acquired 100–3000 m/z; injection volume, 0.2 μL. Collision-induced dissociation (CID) experiments were performed using N_2 as the target gas. The desired double-charged cluster was isolated and subjected to energy-variable CID in which the applied collision energy was raised incrementally. Plots of relative abundance of the parent ion versus applied collision energy were generated with OriginPro 8 SR0 (Microcal Software, Inc., Northampton, MA, USA) to determine $E_{1/2}$ values, which was used as a criterion to evaluate the relative stabilities of the clusters in the gas phase. The dissociation curves were measured in triplicate for each cluster. All data were collected and processed using MassHunter (Agilent Technologies (China) Co., Ltd.) workstation software.

Results and Discussion

The structures of $[Mo_6O_{19}]^{2-}$ (**1**) and its organoimido derivatives (**2**–**10**) were listed in Fig. 1. The negative-ion ESI mass spectra of TBA^+ salts of **1**–**10** dissolved in CH_3CN (Fig.S1 and Table S1 in the supporting information) give well-defined spectra with limited speciation related to the intact, molecular anions $[Mo_6O_{18}(NAr)]^{2-}$ (the most intense peak in all cases), indicating that Lindqvist isopolyanion **1** and its organoimido derivatives (**2**–**10**) maintain their structural integrity in solution. The disubstituted species $[Mo_6O_{17}(NAr)_2]^{2-}$ was also shown in the mass spectra but with relatively weak abundance (ca. < 20%). The CID mass spectra of the arylimido hexamolybdate derivatives (**2**–**10**) versus the parent anion $[Mo_6O_{19}]^{2-}$ (**1**) were presented in Fig. 2 and Table S2 in the supporting information. The precursor ion in each case is shown in a red box. It can be clearly seen that the organoimido-derivatized anions display distinctive fragmentation pattern from its parent species, suggesting that their structural features are different. For example, fragmentation of 1 only generates two molybdate fragments, $[Mo_3O_{10}]^{2-}$ (m/z 223.8340) and $[Mo_4O_{13}]^{2-}$ (m/z 295.7801), presumably via loss of consecutive neutral MoO_3 fragments, respectively, where the molybdenum exists in the highest oxidation state + 6. In contrast, fragmentation of **2**–**10** mainly went through two dissociation pathways (paths A and B, Fig. 3) in which path A generates a variety of low-nuclearity molybdate fragments (mono-, di-, tri-, tetra-, penta-molybdate fragments) with breaking the Mo–N bond, forming a transient radical dianion/neutral complex as an intermediate, followed by the cleavages of the multiple Mo–O bonds resulting in the rupture of POM framework, whereas path B produces a range of low-nuclearity molybdate fragments that retain the organic components via only breaking the multiple Mo–O bonds on POM framework.

The reason why we assume an ion/neutral complex as the intermediate is due to the following facts: (1) the proton source of the protonated molybdate fragments $[H_xMo_yO_z]^{n-}$ (please refer to Fig. 2 and Table S2 in the supporting information) is certainly ascribed to the aromatic amine part by H-abstraction reaction, indicating that the POM anion $[Mo_6O_{19}]^{2-\bullet}$ has a close

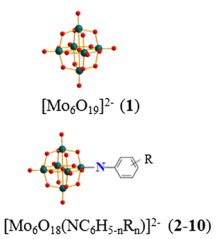

Anion	R	n	m/z	$^aE_{1/2}$ (V)
1	-	-	439.6695	19.81 (31.70)
2	H	1	477.1932	21.41 (23.79)
3	*p*-CH_3	1	484.2011	20.61 (21.14)
4	*o*-CH_3	2	491.2089	20.45 (19.48)
5	*p*-*i*-C_3H_7	1	498.2167	22.05 (19.60)
6	*o*-*i*-C_3H_7	2	519.2403	21.89 (16.21)
7	*p*-OCH_3	1	492.1985	16.09 (16.09)
8	*o*-OCH_3	1	492.1985	16.44 (16.44)
9	*p*-NO_2	1	499.6858	23.81 (25.06)
10	*o*-NO_2	1	499.6858	16.73 (17.61)

$^aE_{1/2}$ values corrected for degrees-of-freedom are given in parentheses.

Figure 1. Ball-and-stick representations of the structures of hexamolybdate $[Mo_6O_{19}]^{2-}$ (**1**) and its arylimido derivatives (**2**–**10**: $[(C_6H_5N)Mo_6O_{18}]^{2-}$ (**2**), $[(p\text{-}CH_3\text{-}C_6H_4N)Mo_6O_{18}]^{2-}$ (**3**), $[(o\text{-}(CH_3)_2\text{-}C_6H_3N)Mo_6O_{18}]^{2-}$ (**4**), $[(p\text{-}i\text{-}C_3H_7\text{-}C_6H_4N)Mo_6O_{18}]^{2-}$ (**5**), $[(o\text{-}(i\text{-}C_3H_7)_2\text{-}C_6H_3N)Mo_6O_{18}]^{2-}$ (**6**), $[(p\text{-}CH_3O\text{-}C_6H_4N)Mo_6O_{18}]^{2-}$ (**7**), $[(o\text{-}CH_3O\text{-}C_6H_4N)Mo_6O_{18}]^{2-}$ (**8**), $[(p\text{-}NO_2\text{-}C_6H_4N)Mo_6O_{18}]^{2-}$ (**9**), and $[(o\text{-}NO_2\text{-}C_6H_4N)Mo_6O_{18}]^{2-}$ (**10**)). The $E_{1/2}$ values for **1**–**10** were listed in the last column; those corrected for degrees-of-freedom were given in parentheses. Color scheme: Mo = teal, N = blue, C = gray, H= dark gray, O = red

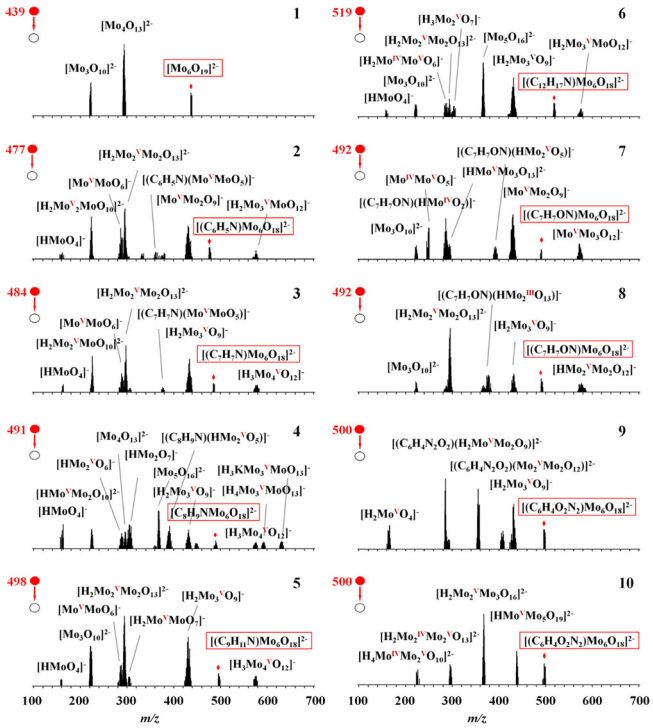

Figure 2. CID mass spectra of the parent molecular anions **1**–**10** at high collision energies (CE), CE = 20 V (**1**), 22 V (**2**), 21 V (**3**), 21 V (**4**), 23 V (**5**), 24 V (**6**), 20 V (**7**), 18 V (**8**), 25 V (**9**), and 18 V (**10**), respectively. The precursor ion in each case is shown in a red box

relationship with the as-formed amine radical; (2) the fact that no discrete $[Mo_6O_{19}]^{2-\bullet}$ fragment via breaking the Mo–N bond in the CID spectra (even when lowering the collision energy to the threshold value where the fragments were just discernible, Fig. S2 in the supporting information) was observed suggests that this species $[Mo_6O_{19}]^{2-\bullet}$ is so unstable that it falls apart into smaller fragments immediately. The main fragments in paths A and B are $[H_2Mo_2{}^{V}Mo_2O_{13}]^{2-}$ (*m/z* 296.7879), $[H_2Mo_2{}^{V}MoO_{10}]^{2-}$ (*m/z* 224.8411), $[Mo^{V}Mo_2O_9]^{-}$ (*m/z* 431.6731), and $[Mo^{V}MoO_6]^{-}$ (*m/z* 287.7802) for **2**; $[H_2Mo_2{}^{V}Mo_2O_{13}]^{2-}$ (*m/z* 296.7875), $[H_2Mo_2{}^{V}MoO_{10}]^{2-}$ (*m/z* 224.8407), and $[H_2Mo_3{}^{V}O_9]^{-}$ (*m/z* 433.6860) for **3**; $[Mo_5O_{16}]^{2-}$ (*m/z* 367.7252), $[HMoO_4]^{-}$ (*m/z* 162.8943), $[HMo^{V}Mo_2O_{10}]^{2-}$ (*m/z* 224.3364), $[HMo_2{}^{V}O_6]^{-}$ (*m/z* 288.7886), $[HMo_2O_7]^{-}$ (*m/z* 304.7854), $[(C_8H_9N)(HMo_2{}^{V}O_5)]^{-}$ (*m/z* 391.8664), and $[H_2Mo_3{}^{V}O_9]^{-}$ (*m/z* 433.6861) for **4**; $[H_2Mo_2{}^{V}Mo_2O_{13}]^{2-}$ (*m/z* 296.7864), $[Mo_3O_{10}]^{2-}$ (*m/z* 223.8340), and $[H_2Mo_3{}^{V}O_9]^{-}$ (*m/z* 433.6860) for **5**; $[Mo_5O_{16}]^{2-}$ (*m/z* 367.7249) and $[H_2Mo_3{}^{V}O_9]^{-}$ (*m/z* 433.6854) for **6**; $[Mo^{V}Mo_2O_9]^{-}$ (*m/z* 431.6772), $[(C_7H_7ON)(HMo^{IV}O_2)]^{-}$ (*m/z* 251.9559), and $[Mo^{V}MoO_6]^{-}$ (*m/z* 287.7825) for **7**; $[H_2Mo_2{}^{V}Mo_2O_{13}]^{2-}$ (*m/z* 296.7879) for **8**; $[(C_6H_4N_2O_2)(H_2Mo^{V}Mo_2O_9)]^{2-}$ (*m/z* 284.8583), $[(C_6H_4N_2O_2)(Mo_2{}^{V}Mo_2O_{12})]^{2-}$ (*m/z* 355.7969), and $[H_2Mo_3{}^{V}O_9]^{-}$ (*m/z* 433.6853) for **9**; and $[H_2Mo_2{}^{V}Mo_3O_{16}]^{2-}$ (*m/z* 368.7307) and $[HMo^{V}Mo_5O_{19}]^{2-}$ (*m/z* 440.1738) for **10**, respectively. The existence of mixed valence molybdate fragments (from + 3 to + 6) may be interpreted as such that Mo^{+6}, having the highest reduction potential, is readily reduced by the as-formed neutral organic amines in the dissociation process, thus generating the mixed-oxidation-state polyoxomolybdate species. This was the first time for the identification of molybdate fragments in reduced oxidation states by tandem mass spectrometry although molybdenum-containing species has been identified in the reduced form previously by examining the ESI-MS spectra of reaction mixtures comprising $[Mo_8O_{26}]^{4-}$ + Mn^{3+} + tris(hydroxymethyl)aminomethane (TRIS) [19] and $[Mo_6O_{19}]^{2-}$ + Ag^{+} [20], respectively. Another important finding in the dissociation study is the presence of molybdate fragments with arylimido group R via breaking the multiple Mo–O bonds on POM framework (path B), manifesting the fact that the Mo–N bond was strengthened via effectively extend the d–π conjugation with the use of substitution effect. The electron withdrawing group such as NO_2 in para position (**9**) is the best example for such kinds of fragments $[(C_6H_4N_2O_2)(H_2Mo^{V}Mo_2O_9)]^{2-}$ (*m/z* 284.8583) and $[(C_6H_4N_2O_2)(Mo_2{}^{V}Mo_2O_{12})]^{2-}$ (*m/z* 355.7969).

Finally, the gas-phase relative stabilities of **2**–**10** versus **1** were evaluated via the $E_{1/2}$ values (defined as the point at which half of the isolated parent ion had dissociated), which were derived from the plots of relative abundance of the parent ion versus applied collisional energy [21, 22]. In the last column of Fig. 1, all the $E_{1/2}$ values in parentheses are adjusted for the degrees of freedom [23] relative to one selected standard, the $[Mo_6O_{18}(NC_6H_3\text{-}p\text{-}(OCH_3))]^{2-}$ (**7**), chosen because all the $E_{1/2}$ values for the other derivatives are higher than this benchmark value. From a structural point of view, the stability of **2**–**10** is essentially determined by the Mo–N bond strength, the only linkage that connects the inorganic and organic segments. Thus, any factors that lessen the Mo–N bond strength will definitely decrease the stability of the molecule as a whole and vice versa since the whole molecule is a large, extended conjugated system resulting from strong d–π interactions. The relative stability decreases in the order of $R = p\text{-}NO_2$ (**9**) > H (**2**) > $p\text{-}CH_3$ (**3**) > $p\text{-}i\text{-}C_3H_7$ (**5**) > $o\text{-}(CH_3)_2$ (**4**) > $o\text{-}NO_2$ (**10**) > $o\text{-}OCH_3$ (**8**) > $o\text{-}(i\text{-}C_3H_7)_2$ (**6**) > $p\text{-}OCH_3$ (**7**). Obviously, substitution effect on the benzene ring plays an important role in the stabilization. $p\text{-}NO_2$ group (electron-withdrawing group) in compound **9** has the best stabilization effect whereas $p\text{-}OCH_3$ (electron-donating group) in the compound **7** influences the stability in the opposite direction. This result may be explained as the fact that the $p\text{-}NO_2$ group can greatly decrease the electron density on the N atom in the Mo–N bond, thus making Mo–N bond less polar and more stable. As for $R = o\text{-}NO_2$ (**10**) and $o\text{-}OCH_3$ (**8**), the O atoms in the nitro and methoxy groups can partially interact with Mo atom in the adjacent Mo–N bond through space to form five- and six-membered rings (Fig. S3 in the supporting information), respectively, which further increase the charge density on the imido-bearing Mo atom, thus demonstrating the least stabilization effect. The alkyl groups ($R = p\text{-}i\text{-}C_3H_7$ (**5**), CH_3 (**3**, **4**), and H (**2**)) as weak electron-donating groups exert minimal impact on molecular stability except for $R = o\text{-}(i\text{-}C_3H_7)_2$ (**6**) where two bulky $i\text{-}C_3H_7$ groups in the adjacent position of aniline block the d–π conjugation

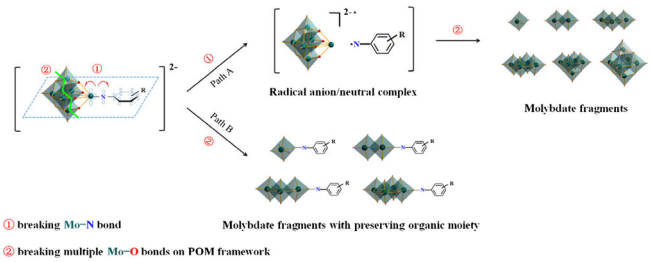

Figure 3. CID fragmentation pathways of **2–10** (color scheme: Mo = teal, N = blue, O = red)

between the benzene ring and POM, thus making it less stable than **2**–**5**. In a word, when the organoimido moiety was introduced onto the framework of $[Mo_6O_{19}]^{2-}$ as a covalent bond, the stability of the resultant arylimido-functionalized POM was determined by the substitution effect on benzene ring.

Conclusion

A series of arylimido-functionalized POMs (**2**–**10**) versus the parent species $[Mo_6O_{19}]^{2-}$ (**1**) was systematically studied by electrospray tandem mass spectrometry. The ESI-MS mass spectra show that **1**–**10** can maintain their structural integrity in solution. The gas-phase fragmentations of **2**–**10** display distinctive fragmentation pattern from **1**, suggesting that their structural features are different. Fragmentation of **1** generates two molybdate fragments only, $[Mo_3O_{10}]^{2-}$ and $[Mo_4O_{13}]^{2-}$, whereas decomposition of **2–10** went through two dissociation pathways in which path A generates a variety of molybdate fragments with breaking the Mo–N bond followed by the cleavages of the multiple Mo–O bonds, whereas path B produces a range of molybdate fragments with arylimido group via solely breaking the multiple Mo-O bonds on POM framework. The existence of mixed valence molybdate fragments suggests that Mo^{+6} is readily reduced in the presence of strong reducing agents. The gas-phase stability order of *R* = *p*-NO_2 (**9**) > H (**2**) > *p*-CH_3 (**3**) > *p*-*i*-C_3H_7 (**5**) > *o*-$(CH_3)_2$ (**4**) > *o*-NO_2 (**10**) > *o*-OCH_3 (**8**) > *o*-(*i*-$C_3H_7)_2$ (**6**) > *p*-OCH_3 (**7**) reveals that substitution effect on the benzene ring plays an important role in stabilizing the whole hybrid clusters.

Acknowledgments

The authors thank the National Natural Science Foundation of China (21371025), the 111 Project (B07012), and the Fundamental Research Grant (20121942006) by the Beijing Institute of Technology (BIT). The authors also thank the Analysis and Testing Center of BIT at Liangxiang campus for providing MS instrument for the analysis.

References

1. Pope, M.T.: Heteropoly and Isopolyoxometalates. Springer-Verlag, Berlin (1983)
2. Hill, C.L.: Progress and challenges in polyoxometalate-based catalysis and catalytic materials chemistry. J. Mol. Catal. A: Chem. **262**, 2–6 (2007)
3. Dolbecq, A., Dumas, E., Mayer, C.R., Mialane, P.: Hybrid Organic-inorganic polyoxometalate compounds: from structural diversity to applications. Chem. Rev. **110**, 6009–6048 (2010)
4. Song, Y.F., Long, D.L., Ritchie, C., Cronin, L.: Nanoscale polyoxometalate-based inorganic/organic hybrids. Chem. Rec. **11**, 158–171 (2011)
5. Zhang, J., Xiao, F.P., Hao, J., Wei, Y.G.: The chemistry of organoimido derivatives of polyoxometalates. Dalton Trans. **41**, 3599–3615 (2012)
6. Vicent, C., Adonin, S.A., Anyushin, A.V., Mainichev, D.A., Sokolov, M.N.: Gas-phase fragmentation reactions of Keggin-type {PW11O39M} (M = Rh, Ir, and Ru) polyoxometalates as fingerprints of the ligands attached at the noble metal site. Eur. J. Inorg. Chem. 5618–5624 (2014)
7. Huang, Y.C., Zhang, J.W., Hao, J., Wei, Y.G.: A general and highly regioselective synthesis approach to multi-functionalized organoimido derivatives of polyoxometalates. Sci. Rep. **6**(24759), 1–10 (2016)
8. Pradeep, C.P., Li, F.Y., Lydon, C., Miras, H.N., Long, D.L., Xu, L., Cronin, L.: Design and synthesis of "dumb-bell" and "triangular" inorganic-organic hybrid nanopolyoxometalate clusters and their characterisation through ESI-MS analyses. Chem. Eur. J. **17**, 7472–7479 (2011)
9. Thiel, J., Yang, D.M., Rosnes, M.H., Liu, X.L., Yvon, C., Kelly, S.E., Song, Y.F., Long, D.L., Cronin, L.: Observing the hierarchical self-assembly and architectural bistability of hybrid molecular metal oxides using ion-mobility mass spectrometry. Angew. Chem. Int. Ed. **50**, 8871–8875 (2011)
10. Song, Y.F., Long, D.L., Kelly, S.E., Cronin, L.: Sorting the assemblies of unsymmetrically covalently functionalized Mn-Anderson polyoxometalate clusters with mass spectrometry. Inorg. Chem. **47**, 9137–9139 (2008)
11. Lau, T.C., Wang, J.Y., Guevremont, R., Siu, K.W.M.: Electrospray tandem mass spectrometry of polyoxoanions. Chem. Commun. 877–878 (1995)
12. Ma, M.T., Waters, T., Beyer, K., Palamarczuk, R., Richardt, P.J.S., O'Hair, R.A.J., Wedd, A.G.: Gas-phase fragmentation of polyoxotungstate anions. Inorg. Chem. **48**, 598–606 (2009)
13. Vila-Nadal, L., Rodriguez-Fortea, A., Yan, L.K., Wilson, E.F., Cronin, L., Poblet, J.M.: Nucleation mechanisms of molecular oxides: a study of the assembly-dissassembly of [W6O19]2− by theory and mass spectrometry. Angew. Chem. Int. Ed. **48**, 5452–5456 (2009)
14. Johnson, G.E., Al Hasan, N.M., Laskin, J.: Influence of Heteroanion and ammonium cation size on the composition and gas-phase fragmentation of polyoxovanadates. Int. J. Mass Spectrom. **354-355**, 333–341 (2013)
15. Al Hasan, N.M., Johnson, G.E., Laskin, J.: Gas-phase synthesis of singly and multiply charged polyoxovanadate anions employing electrospray ionization and collision induced dissociation. J. Am. Soc. Mass Spectrom. **24**, 1385–1395 (2013)
16. Gunaratne, K.D.D., Prabhakaran, V., Johnson, G.E., Laskin, J.: Gas-phase fragmentation pathways of mixed addenda Keggin anions: PMo12-nWnO403− (n = 0−12). J. Am. Soc. Mass Spectrom. **26**, 1027–1035 (2015)
17. Klemperer, W.G.: Tetrabutylammonium isopolyoxometalates. Inorg. Synth. **27**, 74–85 (1992)
18. Wei, Y.G., Xu, B.B., Barnes, C.L., Peng, Z.H.: An efficient and convenient reaction protocol to organoimido derivatives of polyoxometalates. J. Am. Chem. Soc. **123**, 4083–4084 (2001)
19. Wilson, E.F., Miras, H.N., Rosnes, M.H., Cronin, L.: Real-time observation of the self-assembly of hybrid polyoxometalates using mass spectrometry. Angew. Chem. Int. Ed. **50**, 3720–3724 (2011)
20. Wilson, E.F., Abbas, H., Duncombe, B.J., Streb, C., Long, D.L., Cronin, L.: Probing the self-assembly of inorganic cluster architectures in solution with cryospray mass spectrometry: growth of polyoxomolybdate clusters and polymers mediated by silver(I) ions. J. Am. Chem. Soc. **130**, 13876–13884 (2008)
21. Cao, J., Li, C.C., Zhang, Z.X., Xu, C., Yan, J., Cui, F.Y., Hu, C.W.: Intriguing role of a quaternary ammonium cation in the dissociation chemistry of Keggin polyoxometalate anions. J. Am. Soc. Mass Spectrom. **23**, 366–374 (2012)
22. Fan, L.Y., Lin, Z.G., Cao, J., Hu, C.W.: Probing the self-assembly mechanism of lanthanide-containing sandwich-type silicotungstates [{Ln(H2O)n}2{Mn4(B-α-SiW9O34)2(H2O)2}]6− using time-resolved mass spectrometry and X-ray crystallography. Inorg. Chem. **55**, 2900–2908 (2016)
23. David, W.M., Brodbelt, J.S.: Threshold dissociation energies of protonated amine/polyether complexes in a quadrupole ion trap. J. Am. Soc. Mass Spectrom. **14**, 383–392 (2003)